The Virtual Brain links transcranial magnetic stimulation evoked potentials and inhibitory neurotransmitter changes in major depressive disorder

Timo Hofsähs[1,2,*], Marius Pille[1,2], Lucas Kern[1,2,6], Anuja Negi[1,2,3,7], Jil Mona Meier[1,2,*,+], Petra Ritter[1,2,3,4,5,*,+]

1) Berlin Institute of Health at Charité - Universitätsmedizin Berlin, Charitéplatz 1, 10117 Berlin, Germany
2) Charité - Universitätsmedizin Berlin, corporate member of Freie Universität Berlin and Humboldt-Universität zu Berlin, Department of Neurology with Experimental Neurology, Brain Simulation Section, Robert-Koch-Platz 4, 10115 Berlin, Germany
3) Bernstein Focus State Dependencies of Learning and Bernstein Center for Computational Neuroscience, Philippstraße 13, 10117 Berlin, Germany
4) Einstein Center for Neuroscience Berlin, Charitéplatz 1, 10117 Berlin, Germany
5) Einstein Center Digital Future, Wilhelmstraße 67, 10117 Berlin, Germany
6) Current address: FIL Methods Group - Department for Imaging Neuroscience (formerly The Wellcome Centre for Human Neuroimaging), UCL Queen Square Institute of Neurology, University College London, 12 Queen Square, London WC1N 3AR
7) Current address: Technical University Berlin, Straße des 17. Juni 135, 10623 Berlin, Germany

[*] corresponding authors: timo.hofsaehs@charite.de, jil-mona.meier@bih-charite.de, petra.ritter@bih-charite.de

[+] equal contribution, co-last authors

Short/Running Title:

Whole-brain simulations of TMS-evoked potentials in MDD

Keywords:

GABA, Major Depressive Disorder, Neural Mass Model, TEP, TMS, Whole-Brain Simulations

Abstract

Background: Transcranial magnetic stimulation evoked potentials (TEPs) show promise as a biomarker in major depressive disorder (MDD), but the origin of the increased TEP amplitude in these patients remains unclear. Gamma aminobutyric acid (GABA) may be involved, as TEP peak amplitude is known to increase with GABAergic activity, but paradoxically MDD patients exhibit reduced GABA levels. We employed a computational modeling approach to investigate this contradiction.

Methods: Whole-brain simulations in 'The Virtual Brain' (thevirtualbrain.org), employing the Jansen and Rit neural mass model, were optimized to simulate TEPs of healthy individuals (N_{subs}=20, 14 females, 24.5±4.9 years). To mimic MDD, a GABAergic deficit was introduced to the simulations by altering one of two selected inhibitory parameters, the inhibitory synaptic time constant b or the number of inhibitory synapses C_4. The TEP amplitude was quantified and compared for all simulations.

Results: Both parameters, the inhibitory synaptic time constant (r=-0.6, p<0.001) and the number of inhibitory synapses (r=-0.79, p<0.001), showed a significant negative linear correlation to the TEP amplitude. Thus, under local parameter changes, we were able to alter the TEP amplitude towards pathological levels, i.e. creating an MDD-like increase of the global mean field amplitude in line with empirical results.

Conclusions: Our model suggests specific GABAergic deficits as the cause of increased TEP amplitude in MDD patients, which may serve as therapeutic targets. This work highlights the potential of whole-brain simulations in the investigation of neuropsychiatric diseases.

Introduction

Investigative and therapeutic applications of transcranial magnetic stimulation (TMS) in major depressive disorder (MDD) show great, yet insufficiently utilized, potential (1-4). Treatment success of repetitive TMS (rTMS) remains variable (5) and biomarkers lack understanding and standardization (6), fostered by the complexity and elusiveness of MDD pathomechanisms (7). However, the recent success of accelerated rTMS treatment (8, 9) and the potential diagnostic applications of TMS (10) in this high-burden disease (11-13) encourage to deepen the knowledge of TMS effects in MDD patients, paving the way for its broader clinical use.

One piece of the puzzle is the unclear role of the main inhibitory neurotransmitter gamma aminobutyric acid (GABA) in TMS-evoked potentials (TEPs) of MDD patients (14, 15). Higher GABA levels in magnetic resonance spectroscopy (MRS)(16) and pharmacologically induced higher GABA function (17-20) correlate with a higher amplitude of single TEP peaks in healthy controls. The amplitude of TEP peaks in MDD patients is larger than in healthy controls (14, 15) and reduces with rTMS treatment (21-24). However, other results, showing lower GABA levels in MDD patients (25-29), led to the formulation of the GABA hypothesis of depression, which suggests an involvement of a GABAergic deficit in the MDD pathogenesis (30, 31). The question, why lower GABA and higher TEP amplitudes have been shown in MDD patients, while higher GABA function leads to higher TEP peak amplitudes, remains unanswered.

Whole-brain simulations are a versatile investigation tool to gain new insights into brain physiology and pathology, such as neurotransmitter mechanisms (32-35). The open-source software 'The Virtual Brain' (TVB)(36, 37) provides a framework to perform whole-brain simulations for various applications, e.g. to explore physiological brain-network mechanisms (38, 39), investigate disease pathologies (40-42), or simulate neuromodulation techniques (43-45). Further, TVB is currently applied for the first time in a prospective clinical trial for presurgical planning in epilepsy patients (46). For our study,

we make use of the advantages of TVB simulations, by manipulating GABA in individualized whole-brain models to mimic MDD and dissect its effects on TEPs.

Method

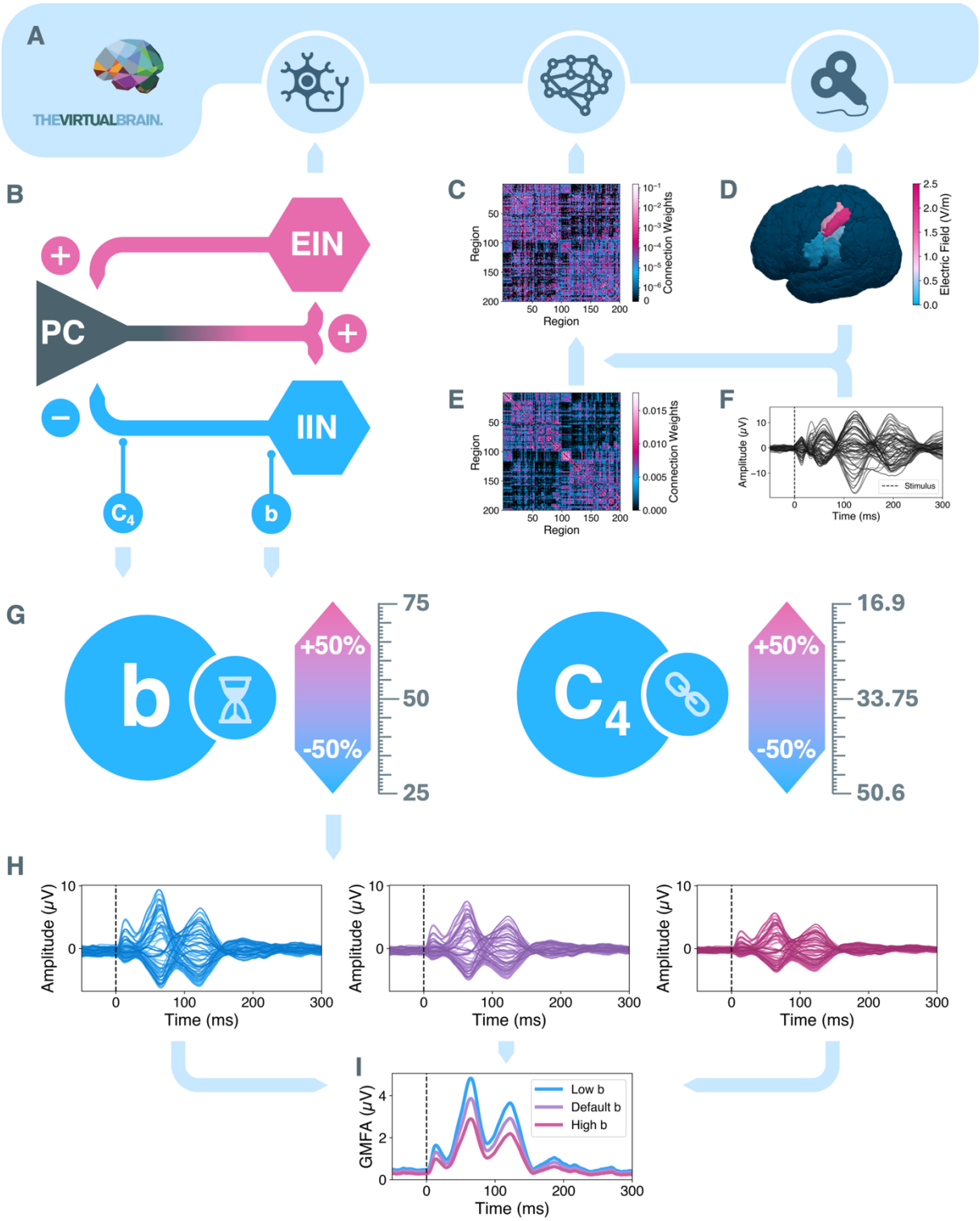

Figure 1: Workflow of the methodological steps. A) Whole-brain simulations with 'The Virtual Brain' were set up. **B)** Neural activity was generated by the Jansen and Rit neural

mass model (47). **C)** The connection weights between all regions were defined in the subject specific optimized structural connectivity (SC) matrix M (depicted for example subject sub-15, diagonal set to 0 for visualization purposes). **D)** Amplitude of transcranial magnetic stimulation of left-hemispheric motor cortex per brain region on a surface brain. Five left-hemispheric regions received stimulation. **E)** Averaged and transformed empirical SC matrix $\widetilde{M}$. To generate simulated transcranial magnetic stimulation evoked potential (TEP) with a high correlation to the empirical TEP **(F)**, the empirical SC matrix $\widetilde{M}$ was optimized, generating subject specific SC matrices M (C). **G)** Whole-brain simulations were repeated with either the inhibitory synaptic time constant b or number of inhibitory synapses C_4 altered to values in the range of -50% to +50% from their default values. **H)** Examples of simulated TEPs for low (left, blue), default (middle, purple) and high (right, magenta) inhibitory synaptic time constant. **I)** The TEP amplitude was quantified by the GMFA. Stimulus onset is marked with a vertical black dashed line in panels (F), (H) and (I). EIN, excitatory interneuron population; GMFA, global mean field amplitude; IIN, inhibitory interneuron population; ms, milliseconds; µV, microvolt; PC, pyramidal cell population; V/m, volt per meter.

Data

An open-access dataset of concurrent electroencephalography (EEG) and TMS (48) was employed to optimize the SCs to generate realistic TEPs of healthy subjects in the whole-brain simulations of this study. The dataset contains 62-channel EEG data of N_{subs}=20 healthy subjects (24.5±4.9 years, 14 females) during single-pulse TMS of the left-hemispheric hand area of the primary motor cortex (M1), averaged over at least 100 repetitions with an intensity of 120% of the resting motor threshold. The empirical TEP timeseries of one example subject is shown in Figure 1F. The original study (49) had been approved by the ethics committee of Monash University, Melbourne, Australia (Nr. CF15/822 - 2015000371). The further data processing for this study received approval by the ethics committee of Charité - Universitätsmedizin Berlin, Germany (Nr. EA4/045/24). A data sharing and processing agreement was set up and signed by the data controllers and processors of this study who worked with the data. For information about the preprocessing of the EEG data, please refer to the original publication (49).

Whole-Brain Simulations with The Virtual Brain

We employed TVB (version 2.7.1) to generate *in-silico* replications of the healthy subject empirical TEPs via whole-brain simulations (50, 51)(Figure 1A, Supplemental Section 'Whole-Brain Simulations', thevirtualbrain.org). Regional brain activity was simulated by one neural mass model per region (NMM, Figure 1B, Section 'Neural Mass Model'). Interaction between all brain regions was defined by their connectome, consisting of region distances and structural connectivity (SC, Figure 1C, Supplemental Section 'Connectome'). The whole-brain simulations were perturbed by virtual TMS (Figure 1D, Supplemental Section 'Virtual TMS'). Simulated EEG timeseries were generated from the simulated source-level timeseries via a forward solution (Supplemental Section 'Forward Solution'). SC matrices were optimized to generate simulated TEPs with a high correlation to empirical TEPs (Figure 1F) by employing a gradient-descent algorithm (52)(Figure 1C-F, Supplemental Section 'Parameter Optimization').

Neural Mass Model

The activity of each brain region was simulated with the NMM by Jansen and Rit (JR)(47). Its ability to generate realistic electrophysiological data and TEPs made it an eligible choice for this work (45, 52, 53). The JR model consists of three neuronal populations, including pyramidal cells (PC), excitatory interneurons (EIN) and inhibitory interneurons (IIN). The PC population is connected to the other populations by two separate feedback loops, while EIN and IIN do not interact directly (Figure 1B, Supplementary Figure S1). The activity of each population is described by the response function and the sigmoidal function. The response function, also known as the rate-to-potential operator, calculates the impulse response in

$$h_{\varepsilon/\iota}(t) = \begin{Bmatrix} H_{\varepsilon/\iota}\frac{t}{\tau_{\varepsilon/\iota}}e^{-\frac{t}{\tau_{\varepsilon/\iota}}},\ t \geq 0 \\ 0,\ t < 0 \end{Bmatrix} \tag{1}$$

for the excitatory populations ε, i.e. PC and IIN, or the inhibitory population ι (Supplemental Figure S2A), i.e. IIN. The function is defined by the maximum postsynaptic potential (PSP) $H_{\varepsilon/\iota}$ and the synaptic time constant $\tau_{\varepsilon/\iota}$, the reciprocal of which represents 'the lumped representation of [...] passive membrane and all other spatially distributed delays in the dendritic network' (47). The response function can be expressed in two first-order linear inhomogeneous differential equations

$$\dot{\upsilon}_j(t) = u_j(t) \tag{2}$$

$$\dot{u}_j(t) = \frac{H_{\varepsilon/\iota}}{\tau_{\varepsilon/\iota}} m_i(t) - \frac{2}{\tau_{\varepsilon/\iota}} u_{\varepsilon/\iota}(t) - \frac{1}{\tau_{\varepsilon/\iota}^2} \upsilon_{\varepsilon/\iota}(t), \tag{3}$$

where the firing rate $m_i(t)$ of the presynaptic region i is applied as input to calculate the mean PSP $\upsilon_j(t)$ of the postsynaptic population j. The sigmoid function S (Supplementary Figure S2B)

$$m_j(\mathrm{t}) = \mathrm{S}\big(\upsilon_\mathrm{j}(\mathrm{t})\big) = \frac{2 \cdot v_{max,j}}{1 + e^{r_j\left(\upsilon_{0,j} - \upsilon_j(t)\right)}} \tag{4}$$

is known as the potential-to-rate operator and calculates the firing rate $m_j(t)$ of a neuronal population j at time point t depending on its mean PSP $\upsilon_j = \sum_i v_{ij}$. Parameter $v_{max,j}$ is half of the maximum of the mean firing rate of population j in spikes per second, $\upsilon_{0,j}$ shows the firing threshold in millivolt for which a 50% firing rate is achieved in population j and the steepness r_j of the curve at the inflection point defines the variability of firing threshold values within the NMM for population j (53). The framework in Equations 1-4 is adapted to each of the three neural populations, resulting in six differential equations. For the NMM in region k, the PSP $y_{0,k}(t)$ of PC is calculated by

$$\dot{y}_{0,k}(t) = y_{3,k}(t) \tag{5}$$

$$\dot{y}_{3,k}(t) = AaS\left(y_{1,k}(t) - y_{2,k}(t)\right) - 2ay_{3,k}(t) - a^2 y_{0,k}(t)\,, \tag{6}$$

the PSP $y_{1,k}(t)$ of EIN with

$$\dot{y}_{1,k}(t) = y_{4,k}(t) \tag{7}$$

$$\dot{y}_{4,k}(t) = Aa\left[C_2 S\left(C_1 y_{0,k}(t)\right) + q_{cou,k}(t) + q_{con} + q_{sti,k}(t) + q_{noi}(t)\right] - 2ay_{4,k}(t) - a^2 y_{1,k}(t) \tag{8}$$

the PSP $y_{2,k}(t)$ of IIN in

$$\dot{y}_{2,k}(t) = y_{5,k}(t) \tag{9}$$

$$\dot{y}_{5,k}(t) = BbC_4 S\left[C_3 y_{0,k}(t)\right] - 2by_{5,k}(t) - b^2 y_{2,k}(t)\,. \tag{10}$$

The general term $H_{\varepsilon/\iota}$ is defined as A in the excitatory populations ε, i.e. PC and EIN, and B in the inhibitory population ι, i.e. IIN. Equivalently, the reciprocal of $\tau_{\varepsilon/\iota}$ is defined as a and b. C_1 and C_2 refer to the number of synapses between PC and EIN and C_3 and C_4 refer to the equivalent between PC and IIN. In Equation 8, which generates the PSP of the EIN, several terms q for additional input are added, including coupled activity from other regions $q_{cou,k}(t)$, constant external input q_{con}, external perturbation $q_{sti,k}(t)$, i.e. TMS, and noise $q_{noi}(t)$. The transformed coupled activity from other regions $q_{cou,k}(t)$ for region k is defined in another sigmoid function

$$q_{cou,k}(t) = g_{min} + \frac{g_{max} - g_{min}}{1 + e^{\frac{-g_a(x_k(t) - g_{mid})}{g_\sigma}}}\,, \tag{11}$$

in which g_{min} and g_{max} define the lower and upper saturation values, g_{mid} defines the midpoint, g_σ the steepness, and g_a the scaling factor. The factor $x_k(t)$ is the summed long-range coupled activity input before transformation through the sigmoid in Equation 11 from all other regions l into region k at time point t and is defined as

$$x_k(t) = \sum_{l=1}^{N_l} M_{kl}\left[y_{1,l}(t - d_{kl}) - y_{2,l}(t - d_{kl})\right], \tag{12}$$

where the PSP per region l is calculated by the difference of state variables $y_{1,l}$ and $y_{2,l}$ at time point t minus the delay d_{kl} between regions k and l, derived by their distance divided by the conduction speed (2.5m/s). The activity is scaled by the individual connection strength between regions k and l, as defined in the optimized SC matrix M (Figure 1C, Supplemental Section 'Parameter Optimization') and summed up over all regions N_l=200 as input for region k. The values for all described parameters are listed in Supplementary Table S1.

Parameter Alteration

After optimizing the SC and simulating healthy control TEPs in TVB utilizing the optimized SC, specific parameters within the whole-brain simulations were altered to introduce GABAergic deficits and assess the impact on TEPs. TEP simulations in TVB were repeated with changed values of b or C_4 (Supplemental Section 'Inhibitory Feedback Loop Analysis'). One of the two parameters was altered to values of -50% to +50% of the respective default values in steps of 2% (b: default=50, range=[25,75]; C_4: default=33.75, range=[16.875,50.625], Figure 1G-H), creating a total of N_{alt}=101 simulations (50 altered values per parameter plus 1 default simulation) per optimized parameter set. Whenever one parameter was altered, the other one was kept at default value. The effect of the maximum and minimum alterations of b and C_4on the JR-inherent functions are shown in Supplementary Figure S2 (A: b alteration effects on the response function; B: C_4 alteration effects on sigmoidal function). For each of the simulations, the global mean field amplitude (GMFA) was calculated to quantify the TEP amplitude (Figure 1I, Supplemental Section 'TEP Amplitude Quantification'). Relative GMFA in percent from default was obtained by division through the GMFA value in the default simulation of the respective individual. For each b and C_4 value the mean over all N_{reps}=100 per subject was calculated to generate the relative GMFA per subject. Then, the mean over these N_{subs}=20 values was taken, resulting in N_{alt}=101 independent mean relative GMFA values, 50 for b, 50 for C_4 and one default value. Two linear regressions were performed, one over the 50

altered values of b plus one default and one over the 50 altered values of C_4 plus one default.

Statistics

The linear relationship between empirical and simulated TEPs was calculated with the Pearson correlation coefficient (PCC) function from the python-library 'SciPy' (54)(Version 1.13.1), providing also a p-value derived using a beta distribution (Supplementary Equation S6). Linear least-squared regression in SciPy was employed to fit a linear model to the relation between mean GMFA and b / C_4 value, which also computes a p-value based on a Wald test. We assumed a significance level of α=0.05 for all tests.

Results

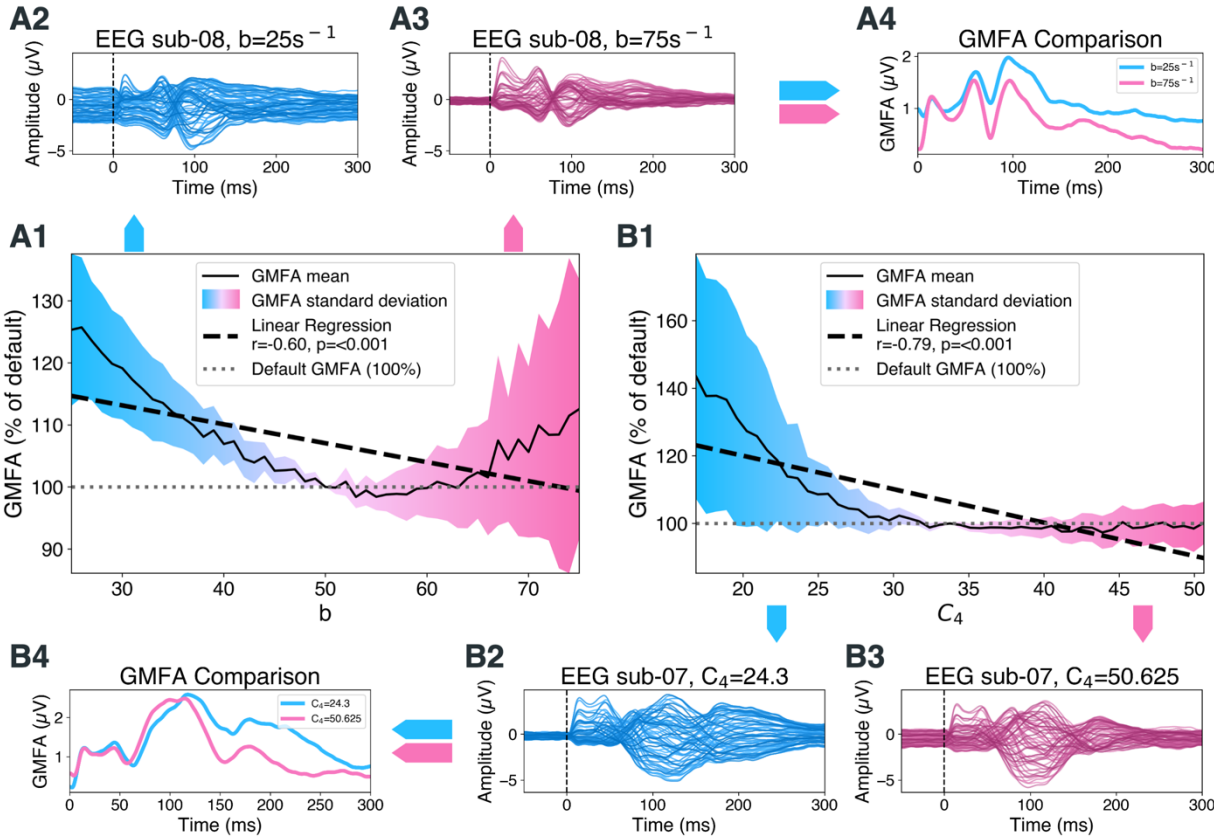

Figure 2: Effects of inhibitory synaptic time constant b and number of inhibitory synapses C_4 on GMFA of transcranial magnetic stimulation evoked potentials. A1) The relative GMFA amplitude (in % relative to GMFA at default parameter value b=50, default is depicted as grey dotted line) per parameter value for b and linear regression is shown here. The solid black line shows the mean relative GMFA over N_{opt}=2,000 optimized parameter sets, the dashed line shows the linear regression calculated over these mean values. The colors indicate the standard deviation of relative GMFA values, i.e. blue for -50% to default and magenta for default to +50%. **A2)** EEG timeseries of example subject sub-08 from a simulation with low inhibitory synaptic time constant (b=25). Each blue line shows the activity measured in one EEG channel. **A3)** EEG timeseries of sub-08 from a simulation with high inhibitory synaptic time constant (b=75). **A4)** Comparison of GMFA from low (b=25, blue) and high (b=75, magenta) inhibitory synaptic time constant simulations for sub-08. **B1-4)** Equivalent plots for the number of inhibitory synapses C4 with example subject sub-07, low C_4=24.3 and high C_4=50.625. Stimulus onset at 0ms is indicated with a vertical black dashed line in panels (A2-3) and (B2-3). EEG, electroencephalography; GMFA, global mean field amplitude; ms, milliseconds; μV, microvolt

An average correlation over all N_{subs}=20 subjects and N_{reps}=100 optimization repetitions between the simulated and empirical TEP timeseries of PCC=0.633 was achieved.

The relations of JR parameters b and C_4 with the relative GMFA of the TEP are depicted in Figure 2. Both the inhibitory time constant b (Figure 2A, r=-0.6, p<0.001) as well as the number of inhibitory synapses C_4 (Figure 2B, r=-0.79, p<0.001) showed a significantly negative linear correlation to the relative GMFA of the overall TEP.

Discussion

In this study, we investigated the role of GABAergic neurotransmission in the genesis of TEP alterations in MDD patients with a whole-brain simulation approach. Our model shows a high correlation between the simulated and empirical TEPs. We were able to alter the TEP amplitude by adjusting the inhibitory time constant and the number of inhibitory synapses.

We reproduced an empirical phenomenon with computational modeling. TEP changes were created through simulation of GABAergic deficits. The TEP amplitude increase was comparable to the one observed empirically in MDD patients, who showed an average TEP amplitude of approximately 130% compared to healthy controls (14). Our findings were achieved in a theory-driven approach by single parameter manipulations, following previous modeling paper approaches (40, 55). This work contributes to the growing number of studies investigating the mechanisms of MDD and possible therapeutic targets through computational whole-brain modeling (44, 56-58).

The results of this study propose a mechanistic connection between two phenomena occurring in MDD patients, GABAergic deficits (30, 31) and an increased TEP amplitude (14, 15). We drew this mechanistic connection by observing TEP amplitude increases after mimicking GABAergic deficits through alterations of local inhibitory model parameters. Thereby, we establish a possible explanation for the previously described open question regarding the mismatch of GABA levels and GABA function in MDD patients. A comparable disconnection of GABA levels and GABA function has previously been reported, as GABA levels assessed with MRS did not correlate with paired-pulse TMS measures in healthy subjects (59). The authors suggested that the methods might measure distinct parts of the GABAergic neurotransmission (59). MRS, for example, mainly measures intracellular concentrations of GABA (25, 60), while paired-pulse TMS measures capture $GABA_A$- and $GABA_B$-receptor dependent function (59). In addition to the existing range of research methods, our *in-silico* approach allows the targeted modulation of GABA function, independent of pharmacological or paired-pulse TMS

approaches. In our simulations, we implemented two separate mechanisms to model reduced GABA function, by reducing the inhibitory synaptic time constant or the number of inhibitory synapses, both leading to increased TEP amplitudes. Hence, our findings appear in contrast with the theory, that increased TEP amplitudes in MDD patients arise from an increased postsynaptic GABA turnover (i.e. higher GABA function but lower GABA levels), which has been postulated in the empirical trials showing increased TEP amplitudes in MDD (14, 15). The TEP amplitude increase might rather arise from higher cortical excitability through lower GABA function, which is disconnected from the relationship of GABA and single TEP peaks.

According to our results, the first mechanism that might cause TEP changes is the disruption of the excitation-inhibition (E/I) timing through alteration of the inhibitory synaptic time constant. More specifically, we demonstrated a linear relationship between this parameter value and the TEP amplitude, i.e. by decreasing the inhibitory synaptic time constant, the average TEP amplitude increased. The inhibitory time constant encompasses all biological processes that affect the speed of neurotransmission in the dendritic network of the IIN (47). Previous studies showed that neurotransmission speed is majorly influenced by the calcium ion dynamics, which evoke the IIN action potential to cause GABA release (61, 62), and the SNARE complex, which fuses the transport vesicle with the IIN cell membrane to release GABA into the postsynaptic cleft (63). GABAergic inhibition physiologically modulates brain activity by determining time windows that allow excitation by inhibiting the postsynaptic membrane potential (64). The TEP captures the physiological, well-timed balance between excitation and inhibition, because it arises from distinct spatiotemporal cascades of excitatory and inhibitory PSPs (65-67). The previously described empirical factors contributing to the inhibitory neurotransmission speed may therefore be involved in MDD pathology and explain both the GABAergic deficit and the increased TEP amplitude.

Our results reveal a second possible explanation of TEP amplitude increases in MDD, which is a decreased number of inhibitory synapses. By lowering the number of inhibitory synapses, a shifted E/I balance with an overweight of excitation is created, causing a TEP

amplitude increase. In line with these findings, a previous study showed an increase in the average PC membrane potential after impairment of the number of inhibitory synapses in a single node model (68). The mathematical parameter for the number of inhibitory synapses may biologically be interpreted as all factors contributing to the hyperpolarizing strength of the IIN on the PC, including the total number of synapses of the IIN onto the PC, the number of functioning postsynaptic $GABA_A$- and $GABA_B$-receptors, the level of GABA concentration in the synaptic cleft, and the postsynaptic ion influx (64, 69). Decreased $GABA_A$- and $GABA_B$-receptor mediated activity has been found in MDD patients in multiple clinical trials (70-73). More generally, an increase in cortical excitability has been shown in MDD patients (74), and previous results have indicated that the vulnerability of GABAergic neurotransmission by IIN might be the main factor disrupting the E/I balance in MDD (73). Our results support these findings and highlight molecular interactions involved in the hyperpolarization strength of IIN within the complex mechanism of inhibition in MDD.

This study contributes to the growing body of literature that is suggesting the GABAergic deficit as a potential target mechanism for MDD therapy (75). Significantly lower GABA concentrations in MDD patients compared to healthy control were found in currently depressed MDD patients, but not in currently remitted MDD patients, suggesting a link between the GABA concentration and depression symptoms (25). Increases in GABA levels were observed following the application of selective serotonin reuptake inhibitors in healthy (76) and depressed subjects (77), and after electroconvulsive therapy in MDD patients (78). Moreover, symptom improvement after rTMS therapy was correlated with an increase in MRS-detected GABA concentration (60) and rTMS therapy has been associated with a decrease in the amplitude of single TEP peaks in multiple studies (21-24). Hence, literature emphasizes the involvement of GABA in the MDD pathology and its restoration by treatment. In line with this, we created digital brain twins of healthy subjects and mimicked a GABAergic deficit through two previously described mechanisms. The model suggests that GABAergic neurotransmission can be targeted to 'reverse' a depressive state to a healthy state, i.e. in terms of a normalization of the TEP amplitude. Corresponding to this, GABA has previously been identified as suitable target

for MDD therapy (75). Novel therapy approaches impacting GABAergic neurotransmission are benzodiazepines, positive allosteric GABA-receptor modulators, ketamine, and rTMS (73, 79-81). Benzodiazepines act via allosteric binding of the postsynaptic $GABA_A$ receptor, which strengthens the GABAergic postsynaptic hyperpolarization (82). Strengthening the GABAergic postsynaptic hyperpolarization was modeled in our simulations by increasing the number of inhibitory synapses. Therefore, the model cannot only be used to draw conclusions about the mechanisms of MDD but provides suggestions for treatment as well. In fact, none of the treatment approaches impacting the GABAergic neurotransmission are currently part of the first-line therapy guidelines in MDD (83), but rTMS has been brought up as a possible first-line approach in MDD, given its promising results and the low success rates of current first-line therapies (84). The results of this study emphasize the potential of tackling the GABAergic deficit for an effective treatment of MDD.

From a dynamical systems perspective, we modeled an emergent network phenomenon by showing the sensitivity of simulated TEPs to local inhibitory parameter alterations. The impact of local inhibitory parameters of the JR model onto neural dynamics in single node non-perturbed models has previously been shown (53, 68). On a network scale, the alterations of local JR parameters can be utilized to investigate complex phenomena, such as integration-segregation (85-87) or dementia (40, 55, 86, 88). In addition, perturbation analysis, in which a system is perturbed by an external stimulus to observe the following effect, is an established method for examining global network dynamics (89, 90). In the simplified two-node network, perturbation-induced dynamics in the JR model are primarily determined by the connectivity strength between the nodes (47, 91-93). Similarly, the response evoked by TMS *in-vivo* is shaped by the network properties, as the activity propagates through diverse pathways over the whole cortex (94). Recent work has modeled these complex network responses to TMS perturbation in healthy subjects (52). In our work, we combined the perturbational approach with local inhibitory JR parameter alterations. The correlation between empirical and simulated TEPs was achieved through SC optimization in our model, confirming the crucial role of the network in the response to TMS perturbation. Moreover, single local inhibitory JR parameter alterations created

global alterations in our whole-brain simulations, mimicking a phenomenon empirically observed in MDD patients.

While this study provides valuable insights, we acknowledge the following limitations. First, the proposed model was not validated with empirical MDD patient data, since, to the best of our knowledge, no suitable open-access dataset was available and attempts to receive non-open data were unsuccessful. A validation against patient data would increase our model's reliability, ideally by linking simulation parameters to depression symptoms. However, our mimicked MDD TEPs were quantitatively compared with empirical published summary results of MDD patients. Additionally, our model focuses specifically on the GABA hypothesis of depression, excluding other relevant hypotheses, such as the monoamine or inflammatory hypotheses (7, 95), which future work utilizing other specified NMM could investigate. Furthermore, spatial details of TMS on a sub-regional level were not considered due to averaging the electric field per region. Moreover, TMS was applied to M1 and not the dorsolateral prefrontal cortex, the area commonly targeted in MDD treatment (96). We chose M1 as stimulation target, because we decided to develop an already validated model further, which was created with the utilized dataset (48) and optimization method (52), and induced GABAergic deficits to model MDD. However, the GABAergic changes were introduced homogeneously over the whole cortex. Further, recent empirical results also proposed M1 as a suitable target for rTMS treatment for MDD, suggesting mechanisms comparable to the dorsolateral prefrontal cortex (97). Lastly, while TEP is a promising biomarker, it has faced criticism due to potential artifacts (98) and the lack of standardized procedures (99).

Neither MDD (95), nor TMS-EEG (4), or GABA in psychiatric disorders (100, 101), are fully understood today. Generally, whole-brain simulations are suitable for targeting open research questions of this intricately linked nature and high complexity level. Additionally, these simulations provide a suitable framework for personalization, a goal shared by psychiatric research in general (102), and TMS research in particular (103-105). Regarding our specific model, future efforts should address the previously described limitations and first and foremost incorporate MDD patient data. Establishing a link between MDD

symptoms and GABAergic alterations could provide additional validity to the model. Another improvement would be the inclusion of a plasticity component (106) to simulate disease progression and investigate the mechanisms of successful therapy as previously proposed (107, 108). Further personalization could be achieved by integrating individual connectomes (109, 110), spatial sub-regional TMS distribution (111), and heterogeneous neurotransmitter maps (35). Ultimately, the goal is to enable pre-therapeutic simulations of MDD patients' brains to optimize stimulation parameters for rTMS treatment.

In this study, we explored the role of GABAergic neurotransmission in the mechanisms underlying increased TEP amplitudes in MDD patients. We optimized whole-brain simulations to generate TEPs of healthy subjects and then modified inhibitory simulation parameters to replicate the GABAergic deficits in MDD. Our findings revealed that lowering the inhibitory synaptic time constant b and the number of inhibitory synapses C_4 led to an increased TEP amplitude. Therefore, this work suggests a mechanistic explanation for TEP alterations in MDD through two separate avenues of altered local inhibition. Future development of novel treatment approaches could consider these pathomechanisms as potential targets. By showcasing our personalized whole-brain modeling approach in this study, our results present a steppingstone towards personalized modeling-enriched MDD therapy in the future.

Acknowledgements

PR acknowledges support by the Virtual Research Environment at the Charité Berlin – a node of EBRAINS Health Data Cloud, by EU Horizon Europe program Horizon EBRAINS2.0 (101147319), Virtual Brain Twin (101137289), EBRAINS-PREP 101079717, AISN – 101057655, EBRAIN-Health 101058516, Digital Europe TEF-Health 101100700, EU H2020 Virtual Brain Cloud 826421, Human Brain Project SGA2 785907; Human Brain Project SGA3 945539, German Research Foundation SFB 1436 (project ID 425899996); SFB 1315 (project ID 327654276); SFB 936 (project ID 178316478; SFB-TRR 295 (project ID 424778381); SPP Computational Connectomics RI 2073/6-1, RI 2073/10-2, RI 2073/9-1; DFG Clinical Research Group BECAUSE-Y 504745852, PHRASE Horizon EIC grant 101058240; Berlin Institute of Health and Foundation Charité. JM acknowledges funding by the Deutsche Forschungsgemeinschaft (DFG, German Research Foundation) – Project-ID 424778381 – TRR 295.

TH and JM acknowledge the use of the large language model 'ChatGPT' (chatgpt.com/) for corrections and improvement of semantics of already written text during the writing process of this script.

Contributions

Conceptualization: TH, JM, PR; Methodology: TH, MP, JM, AN; Software: TH, MP, PR; Validation: TH, JM; Formal Analysis: TH; Investigation: TH, LK; Resources: PR; Data Curation: TH, JM; Writing – Original Draft: TH; Writing – Review & Editing: TH, JM, MP, PR, LK, AN; Visualization: TH; Supervision: JM, PR; Project Administration: JM, PR; Funding Acquisition: PR

We thank current and former members of the 'Brain Simulation Section' at Charité Universitätsmedizin, Berlin, Germany, Halgurd Taher, Jan Stasiński and Chanida Chayopathum for insightful discussions over the course of this project. Computation has

been performed on the High-Performance Cluster for Research and Clinic of the Berlin Institute of Health, Berlin, Germany.

Data and Code Availability

The empirical TEP dataset (48) is publicly available for download (bridges.monash.edu/articles/dataset/TEPs-_SEPs/7440713). The entire code to generate the results presented in this study is openly available (github.com/virtual-twin/TMS_MDD/).

Disclosures

TH, MP, LK, AN, JM and PR all have no financial or other conflicts to declare.

References

1. van Rooij SJH, Arulpragasam AR, McDonald WM, Philip NS (2024): Accelerated TMS - moving quickly into the future of depression treatment. *Neuropsychopharmacology*. 49:128-137.

2. Gonsalves MA, White TL, Barredo J, DeMayo MM, DeLuca E, Harris AD, et al. (2024): Cortical glutamate, Glx, and total N-acetylaspartate: potential biomarkers of repetitive transcranial magnetic stimulation treatment response and outcomes in major depression. *Translational Psychiatry*. 14:5.

3. Fitzsimmons SMDD, Oostra E, Postma TS, van der Werf YD, van den Heuvel OA (2024): Repetitive Transcranial Magnetic Stimulation–Induced Neuroplasticity and the Treatment of Psychiatric Disorders: State of the Evidence and Future Opportunities. *Biological Psychiatry*. 95:592-600.

4. Farzan F (2024): Transcranial Magnetic Stimulation–Electroencephalography for Biomarker Discovery in Psychiatry. *Biological Psychiatry*. 95:564-580.

5. Brunoni AR, Chaimani A, Moffa AH, Razza LB, Gattaz WF, Daskalakis ZJ, et al. (2017): Repetitive Transcranial Magnetic Stimulation for the Acute Treatment of Major Depressive Episodes: A Systematic Review With Network Meta-analysis. *JAMA Psychiatry*. 74:143-152.

6. Julkunen P, Kimiskidis VK, Belardinelli P (2022): Bridging the gap: TMS-EEG from lab to clinic. *Journal of Neuroscience Methods*. 369:109482.

7. Filatova EV, Shadrina MI, Slominsky PA (2021): Major Depression: One Brain, One Disease, One Set of Intertwined Processes. *Cells*. 10.

8. Cole EJ, Phillips AL, Bentzley BS, Stimpson KH, Nejad R, Barmak F, et al. (2022): Stanford Neuromodulation Therapy (SNT): A Double-Blind Randomized Controlled Trial. *Am J Psychiatry*. 179:132-141.

9. Cole EJ, Stimpson KH, Bentzley BS, Gulser M, Cherian K, Tischler C, et al. (2020): Stanford Accelerated Intelligent Neuromodulation Therapy for Treatment-Resistant Depression. *Am J Psychiatry*. 177:716-726.

10. Cao K-X, Ma M-L, Wang C-Z, Iqbal J, Si J-J, Xue Y-X, et al. (2021): TMS-EEG: An emerging tool to study the neurophysiologic biomarkers of psychiatric disorders. *Neuropharmacology*. 197:108574.

11. James SL, Abate D, Abate KH, Abay SM, Abbafati C, Abbasi N, et al. (2018): Global, regional, and national incidence, prevalence, and years lived with disability for 354 diseases and injuries for 195 countries and territories, 1990–2017: a systematic analysis for the Global Burden of Disease Study 2017. *The Lancet*. 392:1789-1858.

12. Vos T, Allen C, Arora M, Barber RM, Bhutta ZA, Brown A, et al. (2016): Global, regional, and national incidence, prevalence, and years lived with disability for 310 diseases and injuries, 1990-2015: a systematic analysis for the Global Burden of Disease Study 2015. *The Lancet*. 388:1545-1602.

13. World Health Organization W (2022): *World mental health report: transforming mental health for all*. Geneva: World Health Organization.

14. Voineskos D, Blumberger DM, Zomorrodi R, Rogasch NC, Farzan F, Foussias G, et al. (2019): Altered Transcranial Magnetic Stimulation-Electroencephalographic Markers of Inhibition and Excitation in the Dorsolateral Prefrontal Cortex in Major Depressive Disorder. *Biol Psychiatry*. 85:477-486.

15. Dhami P, Atluri S, Lee JC, Knyahnytska Y, Croarkin PE, Blumberger DM, et al. (2020): Prefrontal Cortical Reactivity and Connectivity Markers Distinguish Youth Depression from Healthy Youth. *Cereb Cortex*. 30:3884-3894.

16. Du X, Rowland LM, Summerfelt A, Wijtenburg A, Chiappelli J, Wisner K, et al. (2018): TMS evoked N100 reflects local GABA and glutamate balance. *Brain Stimul*. 11:1071-1079.

17. Premoli I, Castellanos N, Rivolta D, Belardinelli P, Bajo R, Zipser C, et al. (2014): TMS-EEG signatures of GABAergic neurotransmission in the human cortex. *J Neurosci*. 34:5603-5612.

18. Premoli I, Biondi A, Carlesso S, Rivolta D, Richardson MP (2017): Lamotrigine and levetiracetam exert a similar modulation of TMS-evoked EEG potentials. *Epilepsia*. 58:42-50.

19. Premoli I, Rivolta D, Espenhahn S, Castellanos N, Belardinelli P, Ziemann U, et al. (2014): Characterization of GABAB-receptor mediated neurotransmission in the human cortex by paired-pulse TMS-EEG. *Neuroimage*. 103:152-162.

20. Darmani G, Zipser CM, Böhmer GM, Deschet K, Müller-Dahlhaus F, Belardinelli P, et al. (2016): Effects of the Selective α5-GABAAR Antagonist S44819 on Excitability in the Human Brain: A TMS-EMG and TMS-EEG Phase I Study. *J Neurosci*. 36:12312-12320.

21. Strafella R, Momi D, Zomorrodi R, Lissemore J, Noda Y, Chen R, et al. (2023): Identifying Neurophysiological Markers of Intermittent Theta-Burst Stimulation in Treatment-Resistant Depression using Transcranial Magnetic Stimulation- Electroencephalography. *Biological Psychiatry*.

22. Voineskos D, Blumberger DM, Rogasch NC, Zomorrodi R, Farzan F, Foussias G, et al. (2021): Neurophysiological effects of repetitive transcranial magnetic stimulation (rTMS) in treatment resistant depression. *Clin Neurophysiol*. 132:2306-2316.

23. Dhami P, Lee J, Schwartzmann B, Knyahnytska Y, Atluri S, Christie GJ, et al. (2022): Neurophysiological impact of theta burst stimulation followed by cognitive exercise in treatment of youth depression. *Journal of Affective Disorders Reports*. 10:100439.

24. Biermann L, Wunram HL, Pokorny L, Breitinger E, Großheinrich N, Jarczok TA, et al. (2022): Changes in the TMS-evoked potential N100 in the dorsolateral prefrontal cortex as a function of depression severity in adolescents. *J Neural Transm (Vienna)*. 129:1339-1352.

25. Godfrey KEM, Gardner AC, Kwon S, Chea W, Muthukumaraswamy SD (2018): Differences in excitatory and inhibitory neurotransmitter levels between depressed patients and healthy controls: A systematic review and meta-analysis. *J Psychiatr Res*. 105:33-44.

26. Gerner RH, Hare TA (1981): CSF GABA in normal subjects and patients with depression, schizophrenia, mania, and anorexia nervosa. *Am J Psychiatry*. 138:1098-1101.

27. Petty F, Sherman AD (1984): Plasma GABA levels in psychiatric illness. *J Affect Disord*. 6:131-138.

28. Rajkowska G, O'Dwyer G, Teleki Z, Stockmeier CA, Miguel-Hidalgo JJ (2007): GABAergic neurons immunoreactive for calcium binding proteins are reduced in the prefrontal cortex in major depression. *Neuropsychopharmacology*. 32:471-482.

29. Hu Y-T, Tan Z-L, Hirjak D, Northoff G (2023): Brain-wide changes in excitation-inhibition balance of major depressive disorder: a systematic review of topographic patterns of GABA- and glutamatergic alterations. *Molecular Psychiatry*. 28:3257-3266.

30. Luscher B, Shen Q, Sahir N (2011): The GABAergic deficit hypothesis of major depressive disorder. *Mol Psychiatry*. 16:383-406.

31. Sanacora G, Mason GF, Rothman DL, Behar KL, Hyder F, Petroff OA, et al. (1999): Reduced cortical gamma-aminobutyric acid levels in depressed patients determined by proton magnetic resonance spectroscopy. *Arch Gen Psychiatry*. 56:1043-1047.

32. Coronel-Oliveros C, Cofré R, Orio P (2021): Cholinergic neuromodulation of inhibitory interneurons facilitates functional integration in whole-brain models. *PLoS Comput Biol*. 17:e1008737.

33. Kringelbach ML, Cruzat J, Cabral J, Knudsen GM, Carhart-Harris R, Whybrow PC, et al. (2020): Dynamic coupling of whole-brain neuronal and neurotransmitter systems. *Proceedings of the National Academy of Sciences*. 117:9566-9576.

34. Naskar A, Vattikonda A, Deco G, Roy D, Banerjee A (2021): Multiscale dynamic mean field (MDMF) model relates resting-state brain dynamics with local cortical excitatory–inhibitory neurotransmitter homeostasis. *Network Neuroscience*. 5:757-782.

35. Deco G, Cruzat J, Cabral J, Knudsen GM, Carhart-Harris RL, Whybrow PC, et al. (2018): Whole-Brain Multimodal Neuroimaging Model Using Serotonin Receptor Maps Explains Non-linear Functional Effects of LSD. *Curr Biol*. 28:3065-3074.e3066.

36. Ritter P, Schirner M, McIntosh AR, Jirsa VK (2013): The virtual brain integrates computational modeling and multimodal neuroimaging. *Brain Connect*. 3:121-145.

37. Sanz-Leon P, Knock SA, Spiegler A, Jirsa VK (2015): Mathematical framework for large-scale brain network modeling in The Virtual Brain. *Neuroimage*. 111:385-430.

38. Koller DP, Schirner M, Ritter P (2024): Human connectome topology directs cortical traveling waves and shapes frequency gradients. *Nature Communications*. 15:3570.

39. Schirner M, Deco G, Ritter P (2023): Learning how network structure shapes decision-making for bio-inspired computing. *Nature Communications*. 14:2963.

40. Stefanovski L, Triebkorn P, Spiegler A, Diaz-Cortes MA, Solodkin A, Jirsa V, et al. (2019): Linking Molecular Pathways and Large-Scale Computational Modeling to Assess Candidate Disease Mechanisms and Pharmacodynamics in Alzheimer's Disease. *Front Comput Neurosci*. 13:54.

41. Falcon MI, Riley JD, Jirsa V, McIntosh AR, Shereen AD, Chen EE, et al. (2015): The Virtual Brain: Modeling Biological Correlates of Recovery after Chronic Stroke. *Frontiers in Neurology*. 6.

42. Courtiol J, Guye M, Bartolomei F, Petkoski S, Jirsa VK (2020): Dynamical Mechanisms of Interictal Resting-State Functional Connectivity in Epilepsy. *The Journal of Neuroscience*. 40:5572-5588.

43. Meier JM, Perdikis D, Blickensdorfer A, Stefanovski L, Liu Q, Maith O, et al. (2022): Virtual deep brain stimulation: Multiscale co-simulation of a spiking basal ganglia model and a whole-brain mean-field model with The Virtual Brain. *Exp Neurol*. 354:114111.

44. An S, Fousek J, Kiss ZHT, Cortese F, van der Wijk G, McAusland LB, et al. (2022): High-resolution virtual brain modeling personalizes deep brain stimulation for treatment-resistant depression: Spatiotemporal response characteristics following stimulation of neural fiber pathways. *NeuroImage*. 249:118848.

45. Kunze T, Hunold A, Haueisen J, Jirsa V, Spiegler A (2016): Transcranial direct current stimulation changes resting state functional connectivity: A large-scale brain network modeling study. *NeuroImage*. 140:174-187.

46. Wang HE, Woodman M, Triebkorn P, Lemarechal JD, Jha J, Dollomaja B, et al. (2023): Delineating epileptogenic networks using brain imaging data and personalized modeling in drug-resistant epilepsy. *Sci Transl Med*. 15:eabp8982.

47. Jansen BH, Rit VG (1995): Electroencephalogram and visual evoked potential generation in a mathematical model of coupled cortical columns. *Biological Cybernetics*. 73:357-366.

48. Biabani M, Rogasch N (2019): TEPs-PEPs. 3 (2019-06-12) ed: Monash University.

49. Biabani M, Fornito A, Mutanen TP, Morrow J, Rogasch NC (2019): Characterizing and minimizing the contribution of sensory inputs to TMS-evoked potentials. *Brain Stimulation*. 12:1537-1552.

50. Schirner M, Domide L, Perdikis D, Triebkorn P, Stefanovski L, Pai R, et al. (2022): Brain simulation as a cloud service: The Virtual Brain on EBRAINS. *Neuroimage*. 251:118973.

51. Sanz Leon P, Knock SA, Woodman MM, Domide L, Mersmann J, McIntosh AR, et al. (2013): The Virtual Brain: a simulator of primate brain network dynamics. *Front Neuroinform*. 7:10.

52. Momi D, Wang Z, Griffiths JD (2023): TMS-evoked responses are driven by recurrent large-scale network dynamics. *Elife*. 12.

53. Spiegler A, Kiebel SJ, Atay FM, Knösche TR (2010): Bifurcation analysis of neural mass models: Impact of extrinsic inputs and dendritic time constants. *Neuroimage*. 52:1041-1058.

54. Virtanen P, Gommers R, Oliphant TE, Haberland M, Reddy T, Cournapeau D, et al. (2020): SciPy 1.0: fundamental algorithms for scientific computing in Python. *Nature Methods*. 17:261-272.

55. Cabrera-Álvarez J, Stefanovski L, Martin L, Susi G, Maestú F, Ritter P (2024): A multiscale closed-loop neurotoxicity model of Alzheimer's disease progression explains functional connectivity alterations. *eneuro*.ENEURO.0345-0323.2023.

56. Escrichs A, Sanz Perl Y, Fisher PM, Martínez-Molina N, G-Guzman E, Frokjaer VG, et al. (2024): Whole-brain turbulent dynamics predict responsiveness to pharmacological treatment in major depressive disorder. *Molecular Psychiatry*.

57. Deco G, Sanz Perl Y, Johnson S, Bourke N, Carhart-Harris RL, Kringelbach ML (2024): Different hierarchical reconfigurations in the brain by psilocybin and escitalopram for depression. *Nature Mental Health*. 2:1096-1110.

58. Wang S, Wen H, Qiu S, Xie P, Qiu J, He H (2022): Driving brain state transitions in major depressive disorder through external stimulation. *Human Brain Mapping*.

59. Cuypers K, Marsman A (2021): Transcranial magnetic stimulation and magnetic resonance spectroscopy: Opportunities for a bimodal approach in human neuroscience. *NeuroImage*. 224:117394.

60. Gonsalves MA, White TL, Barredo J, Fukuda AM, Joyce HE, Harris AD, et al. (2022): Repetitive Transcranial Magnetic Stimulation-Associated Changes in Neocortical Metabolites in Major Depression: A Systematic Review. *Neuroimage Clin*. 35:103049.

61. Sabatini BL, Regehr WG (1996): Timing of neurotransmission at fast synapses in the mammalian brain. *Nature*. 384:170-172.

62. Schneggenburger R, Neher E (2000): Intracellular calcium dependence of transmitter release rates at a fast central synapse. *Nature*. 406:889-893.

63. Acuna C, Guo Q, Burré J, Sharma M, Sun J, Südhof Thomas C (2014): Microsecond Dissection of Neurotransmitter Release: SNARE-Complex Assembly Dictates Speed and Ca2+ Sensitivity. *Neuron*. 82:1088-1100.

64. Pelkey KA, Chittajallu R, Craig MT, Tricoire L, Wester JC, McBain CJ (2017): Hippocampal GABAergic Inhibitory Interneurons. *Physiological Reviews*. 97:1619-1747.

65. Hill AT, Rogasch NC, Fitzgerald PB, Hoy KE (2016): TMS-EEG: A window into the neurophysiological effects of transcranial electrical stimulation in non-motor brain regions. *Neurosci Biobehav Rev*. 64:175-184.

66. Rogasch NC, Fitzgerald PB (2013): Assessing cortical network properties using TMS-EEG. *Hum Brain Mapp*. 34:1652-1669.

67. Tremblay S, Rogasch NC, Premoli I, Blumberger DM, Casarotto S, Chen R, et al. (2019): Clinical utility and prospective of TMS-EEG. *Clin Neurophysiol*. 130:802-844.

68. Wendling F, Bartolomei F, Bellanger JJ, Chauvel P (2002): Epileptic fast activity can be explained by a model of impaired GABAergic dendritic inhibition. *European Journal of Neuroscience*. 15:1499-1508.

69. Schousboe A, Waagepetersen HS (2017): Gamma-Aminobutyric Acid (GABA)☆. *Reference Module in Neuroscience and Biobehavioral Psychology*: Elsevier.

70. Bajbouj M, Lisanby SH, Lang UE, Danker-Hopfe H, Heuser I, Neu P (2006): Evidence for impaired cortical inhibition in patients with unipolar major depression. *Biol Psychiatry*. 59:395-400.

71. Levinson AJ, Fitzgerald PB, Favalli G, Blumberger DM, Daigle M, Daskalakis ZJ (2010): Evidence of cortical inhibitory deficits in major depressive disorder. *Biol Psychiatry*. 67:458-464.

72. Sun Y, Farzan F, Mulsant BH, Rajji TK, Fitzgerald PB, Barr MS, et al. (2016): Indicators for Remission of Suicidal Ideation Following Magnetic Seizure Therapy in Patients With Treatment-Resistant Depression. *JAMA Psychiatry*. 73:337-345.

73. Duman RS, Sanacora G, Krystal JH (2019): Altered Connectivity in Depression: GABA and Glutamate Neurotransmitter Deficits and Reversal by Novel Treatments. *Neuron*. 102:75-90.

74. Kinjo M, Wada M, Nakajima S, Tsugawa S, Nakahara T, Blumberger DM, et al. (2021): Transcranial magnetic stimulation neurophysiology of patients with major depressive disorder: a systematic review and meta-analysis. *Psychol Med*. 51:1-10.

75. Möhler H (2012): The GABA system in anxiety and depression and its therapeutic potential. *Neuropharmacology*. 62:42-53.

76. Bhagwagar Z, Wylezinska M, Taylor M, Jezzard P, Matthews PM, Cowen PJ (2004): Increased brain GABA concentrations following acute administration of a selective serotonin reuptake inhibitor. *Am J Psychiatry*. 161:368-370.

77. Sanacora G, Mason GF, Rothman DL, Krystal JH (2002): Increased occipital cortex GABA concentrations in depressed patients after therapy with selective serotonin reuptake inhibitors. *Am J Psychiatry*. 159:663-665.

78. Sanacora G, Mason GF, Rothman DL, Hyder F, Ciarcia JJ, Ostroff RB, et al. (2003): Increased cortical GABA concentrations in depressed patients receiving ECT. *American Journal of Psychiatry*. 160:577-579.

79. Fogaça MV, Duman RS (2019): Cortical GABAergic Dysfunction in Stress and Depression: New Insights for Therapeutic Interventions. *Front Cell Neurosci*. 13:87.

80. Krystal JH, Kaye AP, Jefferson S, Girgenti MJ, Wilkinson ST, Sanacora G, et al. (2023): Ketamine and the neurobiology of depression: Toward next-generation rapid-acting antidepressant treatments. *Proceedings of the National Academy of Sciences*. 120:e2305772120.

81. Gerhard DM, Pothula S, Liu R-J, Wu M, Li X-Y, Girgenti MJ, et al. (2020): GABA interneurons are the cellular trigger for ketamine's rapid antidepressant actions. *The Journal of clinical investigation*. 130:1336-1349.

82. Griffin CE, 3rd, Kaye AM, Bueno FR, Kaye AD (2013): Benzodiazepine pharmacology and central nervous system-mediated effects. *Ochsner J*. 13:214-223.

83. American Psychological Association A (2019): Clinical practice guideline for the treatment of depression across three age cohorts.

84. O'Sullivan SJ, Buchanan DM, Batail JV, Williams NR (2024): Should rTMS be considered a first-line treatment for major depressive episodes in adults? *Clin Neurophysiol*. 165:76-87.

85. Coronel-Oliveros C, Gießing C, Medel V, Cofré R, Orio P (2023): Whole-brain modeling explains the context-dependent effects of cholinergic neuromodulation. *NeuroImage*. 265:119782.

86. Coronel-Oliveros C, Gómez RG, Ranasinghe K, Sainz-Ballesteros A, Legaz A, Fittipaldi S, et al. (2024): Viscous dynamics associated with hypoexcitation and structural disintegration in neurodegeneration via generative whole-brain modeling. *Alzheimer's & Dementia*. 20:3228-3250.

87. Coronel-Oliveros C, Castro S, Cofré R, Orio P (2021): Structural Features of the Human Connectome That Facilitate the Switching of Brain Dynamics via Noradrenergic Neuromodulation. *Frontiers in Computational Neuroscience*. 15.

88. Triebkorn P, Stefanovski L, Dhindsa K, Diaz-Cortes MA, Bey P, Bülau K, et al. (2022): Brain simulation augments machine-learning-based classification of dementia. *Alzheimers Dement (N Y)*. 8:e12303.

89. Deco G, Cabral J, Saenger VM, Boly M, Tagliazucchi E, Laufs H, et al. (2018): Perturbation of whole-brain dynamics in silico reveals mechanistic differences between brain states. *Neuroimage*. 169:46-56.

90. Gollo LL, Roberts JA, Cocchi L (2017): Mapping how local perturbations influence systems-level brain dynamics. *NeuroImage*. 160:97-112.

91. Basu I, Crocker B, Farnes K, Robertson MM, Paulk AC, Vallejo DI, et al. (2018): A neural mass model to predict electrical stimulation evoked responses in human and non-human primate brain. *J Neural Eng*. 15:066012.

92. Grimbert F, Faugeras O (2006): Bifurcation Analysis of Jansen's Neural Mass Model. *Neural Computation*. 18:3052-3068.

93. Ahmadizadeh S, Karoly PJ, Nešić D, Grayden DB, Cook MJ, Soudry D, et al. (2018): Bifurcation analysis of two coupled Jansen-Rit neural mass models. *PLoS One*. 13:e0192842.

94. Farzan F, Vernet M, Shafi MMD, Rotenberg A, Daskalakis ZJ, Pascual-Leone A (2016): Characterizing and Modulating Brain Circuitry through Transcranial Magnetic Stimulation Combined with Electroencephalography. *Frontiers in Neural Circuits*. 10.

95. Pitsillou E, Bresnehan SM, Kagarakis EA, Wijoyo SJ, Liang J, Hung A, et al. (2020): The cellular and molecular basis of major depressive disorder: towards a unified model for understanding clinical depression. *Molecular Biology Reports*. 47:753-770.

96. Lefaucheur J-P, Aleman A, Baeken C, Benninger DH, Brunelin J, Di Lazzaro V, et al. (2020): Evidence-based guidelines on the therapeutic use of repetitive transcranial magnetic stimulation (rTMS): An update (2014–2018). *Clinical Neurophysiology*. 131:474-528.

97. Hu Y-T, Hu X-W, Han J-F, Zhang J-F, Wang Y-Y, Wolff A, et al. (2024): Motor cortex repetitive transcranial magnetic stimulation in major depressive disorder - A preliminary randomized controlled clinical trial. *Journal of Affective Disorders*. 344:169-175.

98. Conde V, Tomasevic L, Akopian I, Stanek K, Saturnino GB, Thielscher A, et al. (2019): The non-transcranial TMS-evoked potential is an inherent source of ambiguity in TMS-EEG studies. *NeuroImage*. 185:300-312.

99. Belardinelli P, Biabani M, Blumberger DM, Bortoletto M, Casarotto S, David O, et al. (2019): Reproducibility in TMS-EEG studies: A call for data sharing, standard procedures and effective experimental control. *Brain Stimul*. 12:787-790.

100. Fee C, Banasr M, Sibille E (2017): Somatostatin-Positive Gamma-Aminobutyric Acid Interneuron Deficits in Depression: Cortical Microcircuit and Therapeutic Perspectives. *Biological Psychiatry*. 82:549-559.

101. Fries GR, Saldana VA, Finnstein J, Rein T (2023): Molecular pathways of major depressive disorder converge on the synapse. *Molecular Psychiatry*. 28:284-297.

102. Wium-Andersen IK, Vinberg M, Kessing LV, McIntyre RS (2017): Personalized medicine in psychiatry. *Nord J Psychiatry*. 71:12-19.

103. Klooster DCW, Ferguson MA, Boon PAJM, Baeken C (2021): Personalizing Repetitive Transcranial Magnetic Stimulation Parameters for Depression Treatment Using Multimodal Neuroimaging. *Biological Psychiatry: Cognitive Neuroscience and Neuroimaging*.

104. Modak A, Fitzgerald PB (2021): Personalising transcranial magnetic stimulation for depression using neuroimaging: A systematic review. *World J Biol Psychiatry*. 22:647-669.

105. Cocchi L, Zalesky A (2018): Personalized Transcranial Magnetic Stimulation in Psychiatry. *Biological Psychiatry: Cognitive Neuroscience and Neuroimaging*. 3:731-741.

106. Jannati A, Oberman LM, Rotenberg A, Pascual-Leone A (2023): Assessing the mechanisms of brain plasticity by transcranial magnetic stimulation. *Neuropsychopharmacology*. 48:191-208.

107. Wilson MT, Fulcher BD, Fung PK, Robinson PA, Fornito A, Rogasch NC (2018): Biophysical modeling of neural plasticity induced by transcranial magnetic stimulation. *Clin Neurophysiol*. 129:1230-1241.

108. Wilson MT, Fung PK, Robinson PA, Shemmell J, Reynolds JNJ (2016): Calcium dependent plasticity applied to repetitive transcranial magnetic stimulation with a neural field model. *Journal of Computational Neuroscience*. 41:107-125.

109. Triebkorn P, Meier J, Zimmermann J, Stefanovski L, Roy D, Solodkin A, et al. (2024): Fifty shades of The Virtual Brain: Converging optimal working points yield biologically plausible electrophysiological and imaging features. *bioRxiv*.2020.2003.2026.009795.

110. Meier J, Triebkorn P, Schirner M, Ritter P (2024): Connectomes, simultaneous EEG-fMRI resting-state data and brain simulation results from 50 healthy subjects. *bioRxiv*.2024.2004.2017.589718.

111. Thielscher A, Antunes A, Saturnino GB (2015): Field modeling for transcranial magnetic stimulation: A useful tool to understand the physiological effects of TMS? *2015 37th Annual International Conference of the IEEE Engineering in Medicine and Biology Society (EMBC)*, pp 222-225.